Angular distributions for the electron-impact single ionization of sodium and magnesium

G. S. J. Armstrong and J. Colgan
Theoretical Division, Los Alamos National Laboratory, Los Alamos, New Mexico 87545, USA

M. S. Pindzola
Department of Physics, Auburn University, Auburn, Alabama 36849, USA

(Received 6 August 2013; published 29 October 2013)

We present angular distributions for the electron-impact single ionization of sodium and magnesium at intermediate incident electron energies. The results are obtained from a full-dimensionality solution of the two-active-electron time-dependent Schrödinger equation using the time-dependent close-coupling method. We compare calculated angular distributions with existing measurements. We find good overall agreement with measurements over a range of incident electron energies in both cases. We also calculate angular distributions for ejection configurations in which no measurements are currently available.

DOI: 10.1103/PhysRevA.88.042713 PACS number(s): 34.80.Dp

I. INTRODUCTION

The determination of cross sections for the electron-impact ionization of atomic targets is among the most fundamental problems in atomic collision physics. Typically, such cross sections have applications in the astrophysical domain and in transport modeling of plasmas occurring in fusion experiments. Moreover, studies of angular distributions of the outgoing electrons following electron-impact ionization provide highly detailed information on electron-electron correlation and polarization effects in the ionization process. For few-electron systems, such as H and He, a good degree of agreement has been obtained between theory and experiment in predicting total and differential cross sections [1–6]. Some success has also been obtained in predicting angular distributions for electron-impact ionization of H_2 [7–9]. In recent years, a greater emphasis has been placed on the more complex collision dynamics occurring in multielectron systems. A comprehensive set of measured angular distributions is now available for electron-impact ionization of alkali metals [10,11] and noble gases [12]. Recent theoretical studies include convergent close-coupling calculations for Na [13], distorted-wave Born approximation calculations for Na [14–17], K [14], Ca [15], and Mg [16], and *B*-spline *R*-matrix calculations for Ar [18,19] and Ne [20].

The low- and intermediate-impact energy regimes present perhaps the most stringent test of both theory and experiment. In these regimes, experiments must accurately control the electron-beam energy while simultaneously measuring the momenta of the ionizing electrons. For theoretical methods, the challenge lies in the accurate treatment of electron-electron correlation effects, electron-core interactions, and tracking multiple scattering events. Postcollisional interactions between the outgoing electrons play a particularly important role in this domain, and an accurate treatment of such processes is critical to obtain reliable differential cross sections.

In this paper, we present angular distributions for the electron-impact ionization of Na and Mg for a variety of intermediate incident electron energies, calculated using the time-dependent close-coupling (TDCC) method [21]. We make a comparison with available measurements made using the Manchester experimental apparatus [10,11] in both coplanar symmetric and asymmetric geometries. We employ a version of the time-dependent close-coupling approach to electron-impact ionization, where the radial wave function is calculated on a variable radial mesh and propagated in time using an implicit propagator. This approach is important for the accurate treatment of the electron-impact ionization of atoms heavier than He, since a small radial mesh spacing is required to track the rapid oscillations of the radial wave function close to the nucleus. However, away from the nucleus, a larger mesh spacing may be used, and so a variable mesh approach is ideal. Moreover, when used in conjunction with an implicit time propagator, the method proves to be highly efficient, since the time step may take a much larger value than the time step needed for an explicit scheme. Additionally, a core orthogonalization method is used to avoid unphysical deexcitations of the active electrons to any of the filled subshells in the multielectron core during the time propagation.

II. THEORY

A. Time-dependent close-coupling method

Since the current work focuses on single ionization, we treat the incident and ionized electrons as a two-active-electron system, and the interaction with the multielectron core is treated using Hartree-Slater direct and exchange potentials. The two-electron wave function for a given spin S is given as an expansion on a basis set of coupled spherical harmonics, $|l_1 l_2 L\rangle$, of the form

$$\Psi^S(\mathbf{r}_1,\mathbf{r}_2,t) = \sum_{l_1,l_2,L} \frac{P^{LS}_{l_1 l_2}(r_1,r_2,t)}{r_1 r_2} |l_1 l_2 L\rangle. \quad (1)$$

The above expansion may be used to obtain the set of time-dependent close-coupling equations for each LS term, given by

$$i\frac{\partial}{\partial t} P^{LS}_{l_1 l_2}(r_1,r_2,t) = [T_{l_1}(r_1) + T_{l_2}(r_2)] P^{LS}_{l_1 l_2}(r_1,r_2,t) + \sum_{l_1',l_2'} V^{L}_{l_1 l_2, l_1' l_2'}(r_1,r_2) P^{LS}_{l_1' l_2'}(r_1,r_2,t), \quad (2)$$

where $T_l(r)$ is the atomic Hamiltonian, given by

$$T_l(r) = -\frac{1}{2}\frac{\partial^2}{\partial r^2} - \frac{Z}{r} + \frac{l(l+1)}{2r^2} + U_l(r), \tag{3}$$

where Z is the nuclear charge and $U_l(r)$ is an atomic core potential. This potential may be defined as

$$U_l(r) = V_D(r) - \alpha_l\left(\frac{24\rho(r)}{\pi}\right)^{\frac{1}{3}}, \tag{4}$$

where $V_D(r)$ is the direct Hartree potential, α_l is an adjustable parameter, and

$$\rho(r) = \frac{1}{4\pi r^2}\sum_{n,l} w_{nl} P_{nl}^2(r) \tag{5}$$

is the total spherically averaged radial probability density of the core electrons, where $P_{nl}(r)$ is a bound radial orbital for the nl electron of the singly charged ion and w_{nl} is the occupation number. The bound radial orbitals required to construct the atomic core potential $U_l(r)$ are obtained through solution of the Hartree-Fock equations [22] for the singly charged ion. The two-electron term, $V^L_{l_1 l_2, l_1' l_2'}(r_1,r_2)$, is the two-electron repulsion operator. For Na, diagonalization of the one-electron Hamiltonian with $\alpha_0 = 0.505$, $\alpha_1 = 0.55$, and $\alpha_2 = 0.41$ gave a binding energy of -5.1340 eV for the $3s$ orbital, within 0.1% of the measured value of -5.1390 eV [23], and also reproduced the binding energies of the first few higher-lying orbitals to within 0.5% of measured values. For Mg, diagonalization of the one-electron Hamiltonian with $\alpha_0 = 0.48$, $\alpha_1 = 0.55$, and $\alpha_2 = 0.41$ gave a binding energy of -7.6510 eV for the $3s$ orbital, within 0.1% of the measured value of -7.6462 eV [23], and again reproduced the binding energies of the first few higher-lying orbitals to within 0.5% of measured values. This approach provides a reasonable treatment of the interaction of the outgoing electrons with the multielectron core, and has been employed recently to obtain total cross sections for electron-impact ionization of Mg and Al^+ [24] and photoionization of Be and Mg [25].

The two-electron wave function for the initial state is constructed as

$$P^{LS}_{l_1 l_2}(r_1,r_2,t=0) = \sqrt{\frac{1}{2}}\big[G_{k_0 l_1}(r_1)P_{nl_2}(r_2) + (-1)^S P_{nl_1}(r_1)G_{k_0 l_2}(r_2)\big], \tag{6}$$

where k_0 is the linear momentum, $G_{k_0 l}(r)$ is a Gaussian radial wave packet of energy $E_0 = k_0^2/2$, and $P_{nl}(r)$ is a bound radial orbital. The close-coupling equations are then propagated in time for each LS symmetry. During the time propagation, consideration must be given to the possibility of unphysical deexcitation of either of the active electrons to any of the closed subshells of the multielectron core. To avoid this, we use a core-orthogonalization method to prevent deexcitation of the active electrons to any state including $1s$, $2s$, or $2p$ character. For example, the $P^{00}_{00}(r_1,r_2,t)$ radial wave function is orthogonalized at every time step of the propagation of the ^1S state according to

$$\begin{aligned}
P^{00}_{00}(r_1,r_2,t) = {} & P^{00}_{00}(r_1,r_2,t) - P_{1s}(r_1)\int dr_1' P_{1s}(r_1')P^{00}_{00}(r_1',r_2,t) - P_{2s}(r_1)\int dr_1' P_{2s}(r_1')P^{00}_{00}(r_1',r_2,t) \\
& - P_{1s}(r_2)\int dr_2' P_{1s}(r_2')P^{00}_{00}(r_1,r_2',t) - P_{2s}(r_2)\int dr_2' P_{2s}(r_2')P^{00}_{00}(r_1,r_2',t) \\
& + P_{1s}(r_1)P_{1s}(r_2)\int dr_1'\int dr_2' P_{1s}(r_1')P_{1s}(r_2')P^{00}_{00}(r_1',r_2',t) \\
& + P_{1s}(r_1)P_{2s}(r_2)\int dr_1'\int dr_2' P_{1s}(r_1')P_{2s}(r_2')P^{00}_{00}(r_1',r_2',t) \\
& + P_{2s}(r_1)P_{1s}(r_2)\int dr_1'\int dr_2' P_{2s}(r_1')P_{1s}(r_2')P^{00}_{00}(r_1',r_2',t) \\
& + P_{2s}(r_1)P_{2s}(r_2)\int dr_1'\int dr_2' P_{2s}(r_1')P_{2s}(r_2')P^{00}_{00}(r_1',r_2',t).
\end{aligned} \tag{7}$$

Similar expressions may be obtained for all other radial wave functions, where additional projections will be required if either electron is of p character. Following the time propagation of Eq. (2), at a final time $t = T$, the final-state radial wave functions $P^{LS}_{l_1 l_2}(r_1,r_2,T)$ are projected onto products of normalized continuum orbitals of the singly charged ion, $P_{kl}(r)$, to obtain final-state momentum-space wave functions $\mathcal{P}^{LS}_{l_1 l_2}(k_1,k_2,T)$ given by

$$\mathcal{P}^{LS}_{l_1 l_2}(k_1,k_2,T) = \int_0^\infty dr_1 \int_0^\infty dr_2\ P_{k_1 l_1}(r_1)P_{k_2 l_2}(r_2)P^{LS}_{l_1 l_2}(r_1,r_2,T). \tag{8}$$

The continuum orbitals are obtained through solution of the radial one-electron time-independent Schrödinger equation using the direct and exchange potentials defined earlier.

The general form of the triple differential cross section (TDCS) for electron-impact single ionization of atomic targets is

$$\frac{d^3\sigma}{dE_1 d\Omega_1 d\Omega_2} = \frac{w_t}{l_t+1}\frac{\pi}{k_0^2}\frac{1}{k_1 k_2}\sum_S w_S \int_0^\infty dk_1 \int_0^\infty dk_2\ \delta\left[\alpha - \tan^{-1}\left(\frac{k_2}{k_1}\right)\right]|\mathcal{M}|^2, \tag{9}$$

where k_0 is the momentum of the incident electron, k_1 and k_2 are the momenta of the outgoing electrons (ejected into solid angles Ω_1 and Ω_2), α is the hyperspherical angle between k_1 and k_2, and w_t and l_t are the occupation number and angular momentum of the target subshell, respectively. The spin-dependent terms w_S are the appropriate statistical weights of the singlet and triplet states, namely, $w_0 = 1/4$ and $w_1 = 3/4$, and

$$\mathcal{M} = \sum_{l_1,l_2,L} i^L \sqrt{2L+1}(-i)^{l_1+l_2} e^{i(\sigma_{l_1}+\sigma_{l_2})} e^{i(\delta_{l_1}+\delta_{l_2})} \mathcal{P}^{LS}_{l_1 l_2}(k_1,k_2,T)|l_1 l_2 L\rangle. \tag{10}$$

Here, δ_{l_1} and δ_{l_2} are distorted-wave phase shifts, σ_{l_1} and σ_{l_2} are Coulomb phase shifts, and $|l_1 l_2 L\rangle$ is a momentum-space spherical harmonic. The close-coupling equations are propagated in time using an implicit time propagator with time step Δt, according to

$$\begin{aligned} P^{LS}_{l_1 l_2}(r_1,r_2,t+\Delta t) = \sum_{l_1',l_2'} \exp\left[-i\frac{\Delta t}{2} V^L_{l_1 l_2, l_1' l_2'}(r_1,r_2)\right]\left[1+i\frac{\Delta t}{2}T_{l_1'}(r_1)\right]^{-1}\left[1+i\frac{\Delta t}{2}T_{l_2'}(r_2)\right]^{-1} \\ \times\left[1-i\frac{\Delta t}{2}T_{l_2'}(r_2)\right]\left[1-i\frac{\Delta t}{2}T_{l_1'}(r_1)\right]\sum_{l_1'',l_2''}\exp\left[-i\frac{\Delta t}{2}V^L_{l_1' l_2', l_1'' l_2''}(r_1,r_2)\right]P^{LS}_{l_1'' l_2''}(r_1,r_2,t)\,. \end{aligned} \tag{11}$$

This time propagation scheme has previously been used in TDCC studies of the double photoionization of Be and Mg [25] and in the electron-impact ionization of H_2 [7] and H_2^+ [26]. When used in conjunction with a variable mesh finite-difference grid, the implicit propagator has a number of key advantages over an explicit propagator. First, as the radial mesh size is decreased, the time step Δt in the explicit scheme must also be decreased, whereas the time step in the implicit scheme can remain roughly constant and still ensure accurate time propagation. Second, when high angular momenta (l_1,l_2) are included in the calculation, the time step in the implicit scheme can be significantly larger than the time step required in the explicit scheme. This is particularly important for electron-impact ionization of multielectron atoms, where convergence of the close-coupling expansion is typically slower than for smaller atoms such as He.

III. RESULTS

A. Electron-impact ionization of sodium

Calculations pertaining to electron-impact ionization of the Na ground state were carried out at four different incident electron energies between 11.15 and 25.15 eV. At electron-impact energies of 11.15 and 15.15 eV, TDCC calculations were performed using a total of 425 coupled channels, with $0 \leqslant L \leqslant 12$. At 20.15 and 25.15 eV, a total of 513 coupled channels were required for convergence, with $0 \leqslant L \leqslant 14$. A finite-difference grid consisting of $(960)^2$ points with variable mesh spacing $0.01 \leqslant \delta r \leqslant 0.2$ Bohr was used for the radial wave functions. This resulted in a total radial extent of 173.8 Bohr. The radial mesh spacing δr_i between two neighboring points i and $i+1$ was gradually increased according to $\delta r_{i+1} = \delta r_i + 0.001$, until the mesh spacing reached a value of 0.2 Bohr. In Fig. 1, we make a comparison between angular distributions from TDCC calculations and measurements made by the Manchester group [10]. The measurements employ a coplanar symmetric geometry, in which the outgoing electrons are detected in the plane containing the electron beam, and at equal polar angles on either side of the electron beam (i.e., $\theta_1 = \theta_2$, $\phi_1 = \phi_2 = 0^\circ$). In this highly symmetric geometry, the Pauli exclusion principle dictates that only singlet channels contribute to the TDCS in the case of equal energy sharing. In all cases, the relative measurements have been normalized to the TDCC calculations at the peak of the TDCS. At 11.15 eV, the calculated total ionization cross section is 390 Mb, in good agreement with convergent close-coupling (CCC) calculations [27] and in reasonable agreement with measured values of (462 ± 50) Mb [28] and approximately 410 Mb [29]. For each of the incident electron energies shown in Fig. 1, the TDCC calculations are in excellent agreement with experiment over the full range of ejection angles. Over this range of incident electron energies, the angular dependence of the TDCS varies significantly. As incident electron energy is increased, the forward-scattering peak decreases in width and shifts to noticeably lower ejection angles. The backscattering peak appears close to $\theta_2 = 120^\circ$ in all cases, but strongly decreases in magnitude (relative to the forward-scattering peak) as the incident electron energy increases. Between

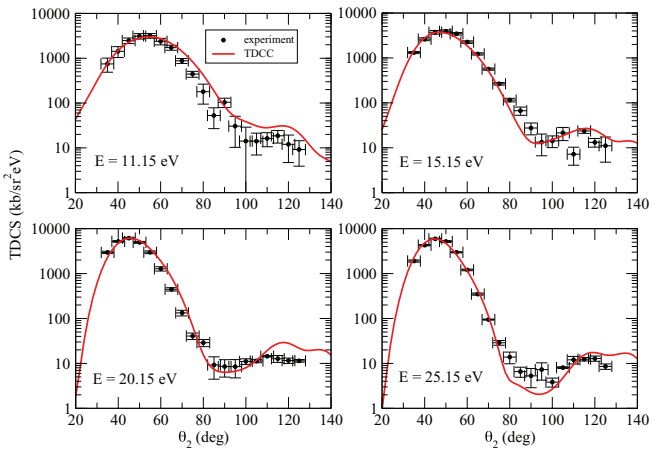

FIG. 1. (Color online) Triple differential cross sections (TDCS) for electron-impact ionization of sodium for equal energy sharing ($E_1 = E_2$) in the coplanar symmetric geometry ($\theta_1 = \theta_2$, $\phi_1 = \phi_2 = 0^\circ$) at four incident electron energies (E), as labeled. We compare with relative measurements [10], which are normalized to the TDCC calculations at the peak of the cross section.

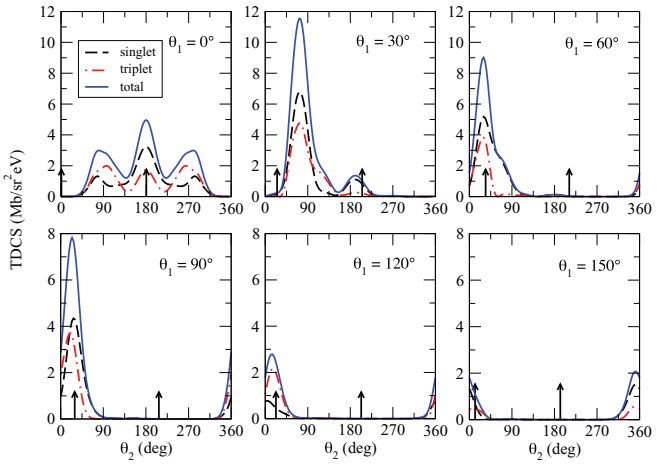

FIG. 2. (Color online) Triple differential cross sections for electron-impact ionization of sodium for equal energy sharing at an incident electron energy of 11.15 eV ($E_1 = E_2 = 3$ eV) in the coplanar asymmetric geometry ($\phi_1 = \phi_2 = 0°$). Note the change of scale in the lower panels. The arrows indicate the positions of the momentum transfer vectors $\mathbf{q}$ and $-\mathbf{q}$.

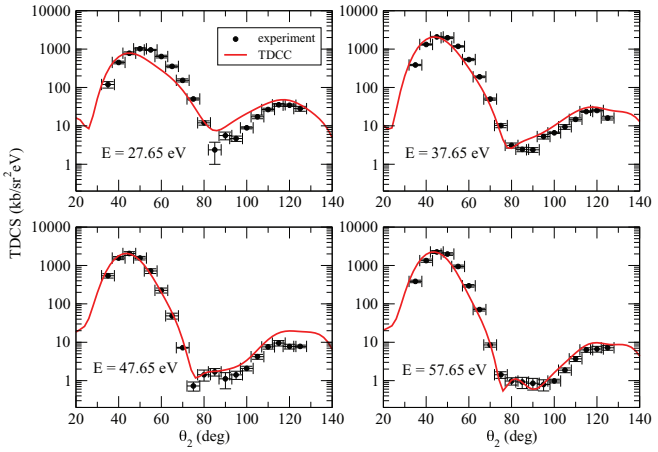

FIG. 3. (Color online) Triple differential cross sections for electron-impact ionization of magnesium for equal energy sharing ($E_1 = E_2$) in the coplanar symmetric geometry ($\theta_1 = \theta_2$, $\phi_1 = \phi_2 = 0°$) at four incident electron energies (E), as labeled. We compare with relative measurements [10], which are normalized to the TDCC calculations at the peak of the theoretical cross section.

these features, an increasingly deep minimum appears. The TDCC calculations reproduce both the angular location and relative magnitudes of these features to a good degree of accuracy, even at the highest electron impact energy where features in the angular distribution span almost four orders of magnitude.

Further information on the ionization dynamics may be obtained by calculating angular distributions in a coplanar asymmetric geometry, where one ejection angle is fixed and the other is varied. No measurements are currently available for Na in such cases, but extensive convergent close-coupling (CCC) calculations have been performed for a wide range of coplanar geometries [13]. In Fig. 2, we show the triple differential cross section for a number of different double ejection configurations at an incident electron energy of 11.15 eV. Both the singlet and triplet contributions to the TDCS appear to be in very good agreement with CCC calculations. As noted in [13], there is a noticeable preference for ejection of one electron at an angle $\theta_1 \simeq 30°$, with the second electron ejected almost perpendicular to the electron beam ($\theta_2 = 90°$). We also note that, when one electron is ejected at a small angle to the electron beam, antiparallel emission ($\theta_2 = \theta_1 + 180°$) tends to make a noticeable contribution to the TDCS. This is particularly evident for $\theta_1 = 0°, 150°$, and to some extent for $\theta_1 = 30°$, where forward scattering provides the dominant contribution. It would be interesting to see new experimental data in this regime to test these predictions.

B. Electron-impact ionization of magnesium

Calculations pertaining to electron-impact ionization of the Mg ground state were carried out at four different incident electron energies between 27.65 and 57.65 eV. In all cases, a total of 524 coupled channels were required for convergence, with $0 \leqslant L \leqslant 14$. These calculations used the same variable radial mesh as was used for the Na calculations.

In Fig. 3, we make a comparison between angular distributions from TDCC calculations and measurements made by the Manchester group [10] for electron-impact ionization of Mg in coplanar symmetric geometry. In all cases shown in Fig. 3, the TDCC calculations are in good agreement with experiment over the full range of ejection angles θ_2. The level of agreement between the calculations and measurements appears to improve slightly as the incident electron energy increases. At $E = 27.65$ eV, the forward-scattering peak in the calculations appears at a lower ejection angle than in the measurements, and the calculations tend to underestimate the magnitude of the TDCS for $\theta_2 < 70°$. The angular position of the minimum is well reproduced, but is now larger in magnitude than the measured value. The angular position of the backscattering peak is in excellent agreement with experiment. The discrepancies observed in this case may be due to an incomplete treatment of correlation in the doubly occupied valence shell. At the same excess energy of 20 eV, the measured TDCS for Na in this geometry was accurately reproduced, as shown in Fig. 1. In all other cases, the angular position and width of the measured forward-scattering peak is well reproduced in the calculations. It is possible that as incident electron energy increases, the more rapid ejection of the $3s$ electron reduces the sensitivity of the TDCS to valence-shell correlation. Sensitivity to such correlation can only be tested using a three-electron calculation, in which both valence-shell electrons are considered to play an active role in the dynamics, although only one is ionized. However, both the calculation of three-electron wave functions and the extraction of angular distributions are highly challenging from a computational standpoint. The convergence with respect to the number of coupled channels is generally slow, and large radial grids are required to calculate accurate radial wave functions for low-energy scattering.

In the remaining cases, the position and relative magnitude of the minimum at around $\theta_2 = 75°$ are in excellent agreement with the measurement for each case. At $E = 57.65$ eV, the

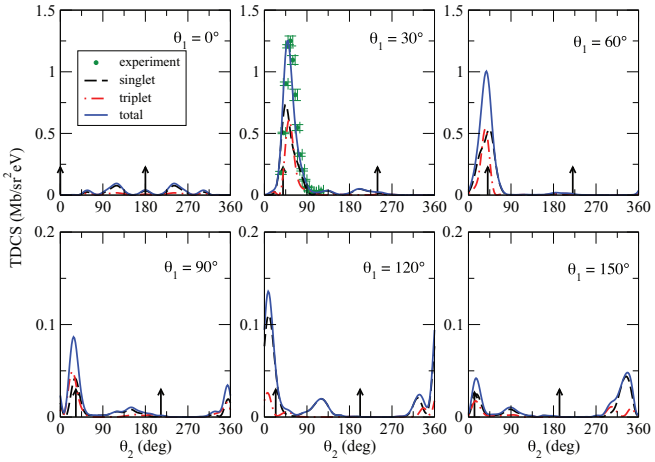

FIG. 4. (Color online) Triple differential cross sections for electron-impact ionization of magnesium for equal energy sharing at an incident electron energy of 47.65 eV ($E_1 = E_2 = 20$ eV), in the coplanar asymmetric geometry ($\phi_1 = \phi_2 = 0^\circ$). We compare with measurements presented in [11]. Note the change of scale in the lower panels. The arrows indicate the positions of the momentum transfer vectors $\mathbf{q}$ and $-\mathbf{q}$.

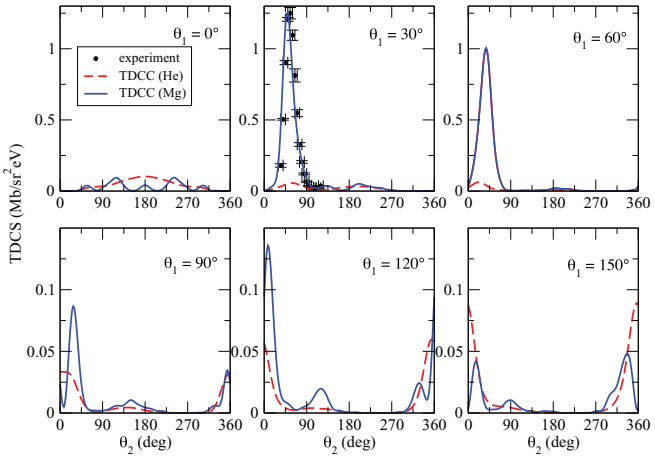

FIG. 5. (Color online) Triple differential cross sections for electron-impact ionization of magnesium for equal energy sharing at an incident electron energy of 47.65 eV ($E_1 = E_2 = 20$ eV), in the coplanar asymmetric geometry ($\phi_1 = \phi_2 = 0^\circ$). We compare with measurements presented in [11] and with TDCC calculations for He at incident electron energy of 64.6 eV ($E_1 = E_2 = 20$ eV). Note the change of scale in the lower panels.

TDCC calculations are also able to match measured features close to the minimum whose magnitude is several orders lower than the forward-scattering peak. The position of the calculated backscattering peak is in good agreement with measurements in all cases. The calculations also accurately predict the relative magnitude of the backscattering peak, with the slight exception of $E = 47.65$ eV, where the calculations overestimate the magnitude by a small amount. We find that, at 47.65 eV, the calculated total cross section of 275 Mb is in good agreement with previous TDCC and R-matrix with pseudostates calculations, but somewhat lower than measured values [24].

In Fig. 4, we show angular distributions calculated at an incident electron energy of 47.65 eV for a coplanar asymmetric geometry, in which the ejection angle of one electron is held fixed while the other is varied. For $\theta_1 = 30^\circ$, we make a comparison with previous measurements given in [11]. In this case, the TDCC calculation is generally in good agreement with experiment. The position of the calculated forward-scattering peak close to $\theta_2 = 45^\circ$ is approximately 5° lower than in the measurement, although this is within the experimental range of uncertainty. The measured position and relative magnitude of the minimum close to $\theta_2 = 100^\circ$ are again well reproduced in the calculations. As in the case of Na, we find a strong preference for ejection of one electron at an angle $30^\circ < \theta_1 < 60^\circ$. However, in the case of Mg, the second electron is predominantly emitted at an angle close to $\theta_2 = 45^\circ$ for both $\theta_1 = 30^\circ$ and $\theta_1 = 60^\circ$. For Na, the forward-scattering peaks occur at $\theta_2 = 75^\circ$ and $\theta_2 = 35^\circ$, respectively, in these two cases. This change in the angular location of the forward-scattering peak is likely due to both the increase in incident electron energy and the differing core-valence interactions in Na and Mg. We note that, in addition to some variation in the forward-scattering peak position, additional structure is observed in the TDCS for Mg compared to those obtained for Na. We also note significant differences in the balance between singlet and triplet contributions to the respective angular distributions for Na and Mg. As is to be expected, for $\theta_1 = 0^\circ$, the relative contribution of antiparallel emission ($\theta_2 = 180^\circ$) has decreased in comparison to the results of Fig. 2, due to the increased incident electron energy, which ought to reduce the effect of any dynamics mediated by electron-electron repulsion.

Finally, in the case of Mg, where a single $3s$ electron is ionized from a closed $3s^2$ shell, it is instructive to make a comparison with angular distributions for ionization of He (for the same final kinematics), where a $1s$ electron is ionized from a closed $1s^2$ shell. In Fig. 5, we compare TDCC calculations for Mg at an incident electron energy of 47.65 eV with those for He at an incident electron energy of 64.6 eV (i.e., a common excess energy of 40 eV). The TDCC calculations for He are similar to those described in [2] and are in good agreement with previous CCC calculations [30]. For $\theta_1 = 0^\circ$, the He TDCS shows a slight preference for antiparallel emission, although emissions at other angles make sizable contributions. For Mg, the dominant emission configurations are more strongly marked by relatively narrow peaks at $\theta_2 = 60^\circ$, 120°, 180°, 240°, and 300°. The magnitude of the strongest peak in each of the distributions is approximately equal. However, for $\theta_1 = 30^\circ$, a large difference in the respective TDCS magnitudes becomes apparent. As noted previously, the Mg TDCS displays a strong preference for this emission configuration, whereas the He TDCS decreases in magnitude as θ_1 is increased from 0° to 30°. For Mg, the forward-scattering peak occurs at a lower angle and also dominates the TDCS to a greater degree than for He. The backscatter peak occurs at a similar angle to that observed in He. For $\theta_1 = 60^\circ$, a similar difference in magnitude is again observed between the respective angular distributions. The forward-scattering peak for Mg is now at a larger angle than for He, while the backscattering peak is again in a similar position close to 180° in both cases. For $\theta_1 = 90^\circ$, the respective angular distributions are now of a

similar magnitude, mainly due to the sharp decrease in the Mg TDCS as θ_1 is increased from 60° to 90°. Here, the main difference lies in the nature of the forward-scattering peak, which in He appears as a broad peak centered close to $\theta_2 = 0°$. For Mg, two peaks appear, one close to $\theta_2 = 0°$ and a larger peak close to $\theta_2 = 40°$. A similar double-peak structure is observed in the Mg TDCS for $\theta_1 = 120°$ and $\theta_1 = 150°$, where the He TDCS continues to display a single peak centered close to $\theta_2 = 0°$. In these cases, the high mutual angle between the outgoing electrons reduces the Coulomb interaction, and therefore interactions with the multielectron core should become more dominant. It is possible in these cases that the double-peak structure in the Mg TDCS occurs due to a greater degree of interplay between the electron-electron and electron-core interactions in a multielectron atom. The richer structure in the angular distributions from the multielectron atom has also been observed in comparisons of the double photoionization of Be and He [31].

The respective characters of the angular distributions for He and Mg naturally depend on the differing core-valence interactions and the differing radial extents of the valence shells. The noticeable dominance of forward scattering in the Mg TDCS is likely due to the diffuse (compared to He) nature of the Mg valence shell. This trend has been observed previously when comparing angular distributions for H and Na [13]. More general differences in the TDCS angular features are likely to be caused by both the differing nature of the inactive He^+ and Mg^+ cores and the differing characters of the ionized $1s$ electron from He compared to the $3s$ electron from Mg, which has more radial nodes.

IV. SUMMARY

In this paper, we have used a version of the time-dependent close-coupling method to calculate differential cross sections for electron-impact ionization of the Na and Mg atoms. Use of an implicit time propagation scheme allows the two-electron wave function to be tracked on a fine variable radial mesh in a highly efficient manner. A core-orthogonalization method is used to prevent unphysical deexcitation of the active electrons to filled core subshells during the time propagation. We have demonstrated that the method is able to determine accurate triple differential cross sections for electron-impact ionization of multielectron atoms over a range of intermediate impact energies. We have performed further calculations of triple differential cross sections for Na and Mg where no experimental data is currently available. We have made a further comparison between the angular distributions for Mg and He for the same final kinematics. This comparison has uncovered features in the Mg TDCS that are not seen in the case of He. We observe a double-peak structure in the Mg TDCS when one electron is ejected at 90° or more to the electron beam. This effect may be due to the influence of the multielectron core in Mg, which competes with the Coulomb interaction between the outgoing electrons to a greater degree than in He. We plan to extend the calculations presented here to the case of electron-impact ionization of the first excited state of Mg. Recent experiments have measured the TDCS for the $[Ne]3s3p\ ^1P$ state of Mg, and are also able to vary the alignment of the $3p$ orbital using a dye laser. Here, the anisotropy of the target coupled with its rotation both in and out of the detection plane ought to facilitate interesting collisional dynamics. The version of the TDCC method presented here will be ideal for this task, since a much larger number of couplings will be required to describe the intricate dynamical response of the excited state target. The efficient use of a variable radial mesh and implicit time propagation should make this problem more tractable. We also plan to use the three-electron TDCC method to investigate valence-shell correlation effects in this complex problem.

ACKNOWLEDGMENTS

The Los Alamos National Laboratory is operated by Los Alamos National Security, LLC for the National Nuclear Security Administration of the U.S. Department of Energy under Contract No. DE-AC5206NA25396. Computational work was carried out at Los Alamos National Laboratory through the provision of an Institutional Computing Resources award. This work was supported in part by grants from the U.S. DOE and U.S. NSF to Auburn University. We thank K. L. Nixon and A. J. Murray for useful discussions.

[1] J. Colgan, M. Foster, M. S. Pindzola, I. Bray, A. T. Stelbovics, and D. V. Fursa, J. Phys. B: At. Mol. Opt. Phys. **42**, 145002 (2009).
[2] J. Colgan, M. S. Pindzola, G. Childers, and M. A. Khakoo, Phys. Rev. A **73**, 042710 (2006).
[3] J. Colgan and M. S. Pindzola, Phys. Rev. A **74**, 012713 (2006).
[4] X. Ren, I. Bray, D. V. Fursa, J. Colgan, M. S. Pindzola, T. Pflüger, A. Senftleben, S. Xu, A. Dorn, and J. Ullrich, Phys. Rev. A **83**, 052711 (2011).
[5] I. Bray and D. V. Fursa, J. Phys. B: At. Mol. Opt. Phys. **44**, 061001 (2011).
[6] O. Zatsarinny and K. Bartschat, Phys. Rev. A **85**, 062709 (2012).
[7] J. Colgan, M. S. Pindzola, F. Robicheaux, C. Kaiser, A. J. Murray, and D. H. Madison, Phys. Rev. Lett. **101**, 233201 (2008).
[8] J. Colgan, O. Al-Hagan, D. H. Madison, C. Kaiser, A. J. Murray, and M. S. Pindzola, Phys. Rev. A **79**, 052704 (2009).
[9] O. Al-Hagan, C. Kaiser, D. H. Madison, and A. J. Murray, Nat. Phys. **5**, 59 (2009).
[10] A. J. Murray, Phys. Rev. A **72**, 062711 (2005).
[11] K. L. Nixon and A. J. Murray, Phys. Rev. Lett. **106**, 123201 (2011).
[12] K. L. Nixon and A. J. Murray, Phys. Rev. A **87**, 022712 (2013).
[13] I. Bray, D. V. Fursa, and A. T. Stelbovics, J. Phys. B: At. Mol. Opt. Phys. **41**, 215203 (2008).
[14] M. K. Srivastava, R. K. Chauhan, and R. Srivastava, Phys. Rev. A **74**, 064701 (2006).
[15] Y. Khajuria and P. C. Deshmukh, Phys. Rev. A **78**, 024702 (2008).

[16] U. Hitawala, G. Purohit, and K. K. Sud, J. Phys. B: At. Mol. Opt. Phys. **41**, 035205 (2008).
[17] Y. Wang, L. Jiao, and Y. Zhou, Phys. Lett. A **376**, 2122 (2012).
[18] X. Ren, T. Pflüger, J. Ullrich, O. Zatsarinny, K. Bartschat, D. H. Madison, and A. Dorn, Phys. Rev. A **85**, 032702 (2012).
[19] O. Zatsarinny and K. Bartschat, Phys. Rev. A **85**, 032708 (2012).
[20] T. Pflüger, O. Zatsarinny, K. Bartschat, A. Senftleben, X. Ren, J. Ullrich, and A. Dorn, Phys. Rev. Lett. **110**, 153202 (2013).
[21] J. Colgan and M. S. Pindzola, Eur. J. Phys. D **66**, 284 (2012).
[22] C. Froese Fischer, Comput. Phys. Commun. **43**, 355 (1987).
[23] See http://physics.nist.gov/PhysRefData/ASD (unpublished).
[24] J. A. Ludlow, C. P. Ballance, S. D. Loch, M. S. Pindzola, and D. C. Griffin, Phys. Rev. A **79**, 032715 (2009).
[25] M. S. Pindzola, C. P. Ballance, Sh. A. Abdel-Naby, F. Robicheaux, G. S. J. Armstrong, and J. Colgan, J. Phys. B: At. Mol. Opt. Phys. **46**, 035201 (2012).
[26] M. S. Pindzola, F. Robicheaux, and J. Colgan, J. Phys. B: At. Mol. Opt. Phys. **38**, L285 (2005).
[27] I. Bray, Phys. Rev. Lett. **73**, 1088 (1994).
[28] A. R. Johnston and P. D. Burrow, Phys. Rev. A **51**, R1735 (1995).
[29] K. Fuji and S. K. Srivastava, J. Phys. B: At. Mol. Opt. Phys. **28**, L559 (1995).
[30] I. Bray, T. Lepage, D. V. Fursa, and A. T. Stelbovics, J. Phys. B: At. Mol. Opt. Phys. **43**, 074028 (2010).
[31] J. Colgan and M. S. Pindzola, Phys. Rev. A **65**, 022709 (2002).